

Supporting Information for:

## Selective Binding of O<sub>2</sub> over N<sub>2</sub> in a Redox-Active Metal-Organic Framework with Open Iron(II) Coordination Sites

Eric D. Bloch,<sup>a</sup> Leslie J. Murray,<sup>a,c</sup> Wendy L. Queen,<sup>d</sup> Sachin Chavan,<sup>e</sup> Sergey N. Maximoff,<sup>b</sup> Julian P. Bigi,<sup>a</sup> Rajamani Krishna,<sup>f</sup> Vanessa K. Peterson,<sup>g</sup> Fernande Grandjean,<sup>h</sup> Gary J. Long,<sup>i</sup> Berend Smit,<sup>b</sup> Silvia Bordiga,<sup>e</sup> Craig M. Brown,<sup>d,g</sup> and Jeffrey R. Long<sup>\*,a</sup>

<sup>a</sup>Department of Chemistry and <sup>b</sup>Department of Chemical and Biomolecular Engineering, University of California, Berkeley, California 94720, USA, <sup>c</sup>Department of Chemistry, University of Florida, Gainesville, Florida 32611, USA, <sup>d</sup>National Institute of Standards and Technology, Center for Neutron Research, Gaithersburg, Maryland 20899, USA, <sup>e</sup>Department of Inorganic, Physical, and Materials Chemistry, NIS Centre of Excellence and INSTM Centre of Reference, University of Turin, Via Quarelo 11, I-10135, Torino, Italy, <sup>f</sup>Van't Hoff Institute for Molecular Sciences, University of Amsterdam, Science Park 904, 1098 XH Amsterdam, The Netherlands, <sup>g</sup>The Bragg Institute, Australian Nuclear Science and Technology Organisation, PMB1, Menai, NSW, Australia, <sup>h</sup>Faculty of Sciences, University of Liège, B-4000 Sart-Tilman, Belgium, <sup>i</sup>Department of Chemistry, Missouri University of Science and Technology, University of Missouri, Rolla, Missouri 65409-0010, USA.

*J. Am. Chem. Soc.*

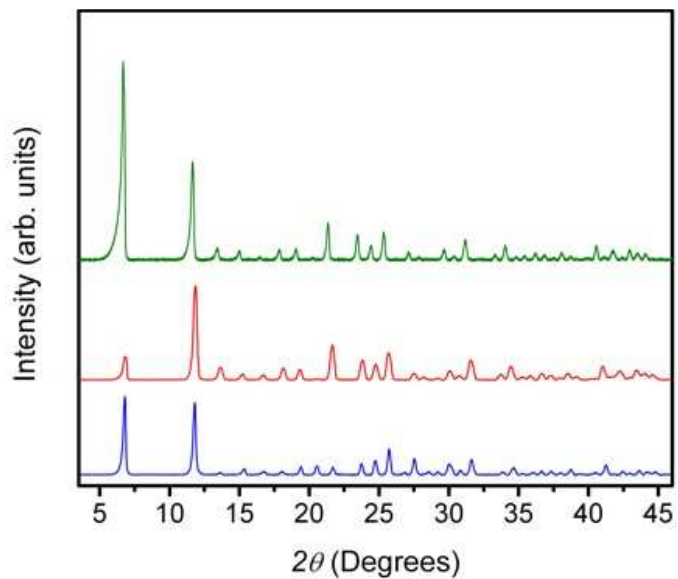


**Figure S1.** Comparison between the powder X-ray diffraction patterns of as-synthesized  $\text{Fe}_2(\text{dobdc})$  (green),  $\text{Zn}_2(\text{dobdc})$  (red), and  $\text{Mg}_2(\text{dobdc})$  (blue).

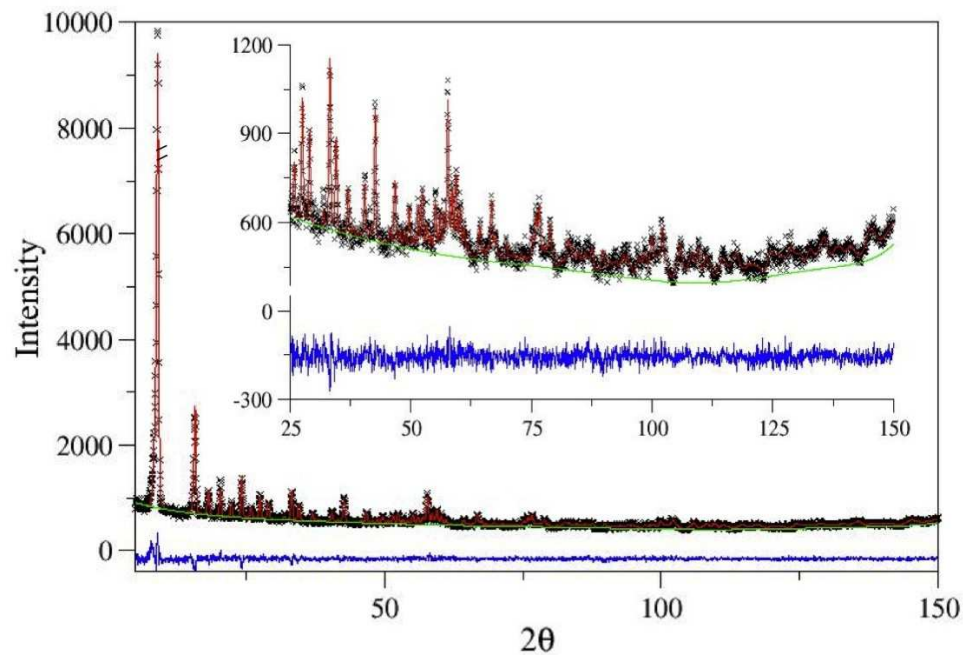


**Figure S2.** Rietveld refinement of the experimental neutron diffraction pattern of desolvated  $\text{Fe}_2(\text{dobdc})$ . The calculated pattern (red line) is in good agreement with the experimental data (crosses) as evidenced by the difference pattern (blue line)

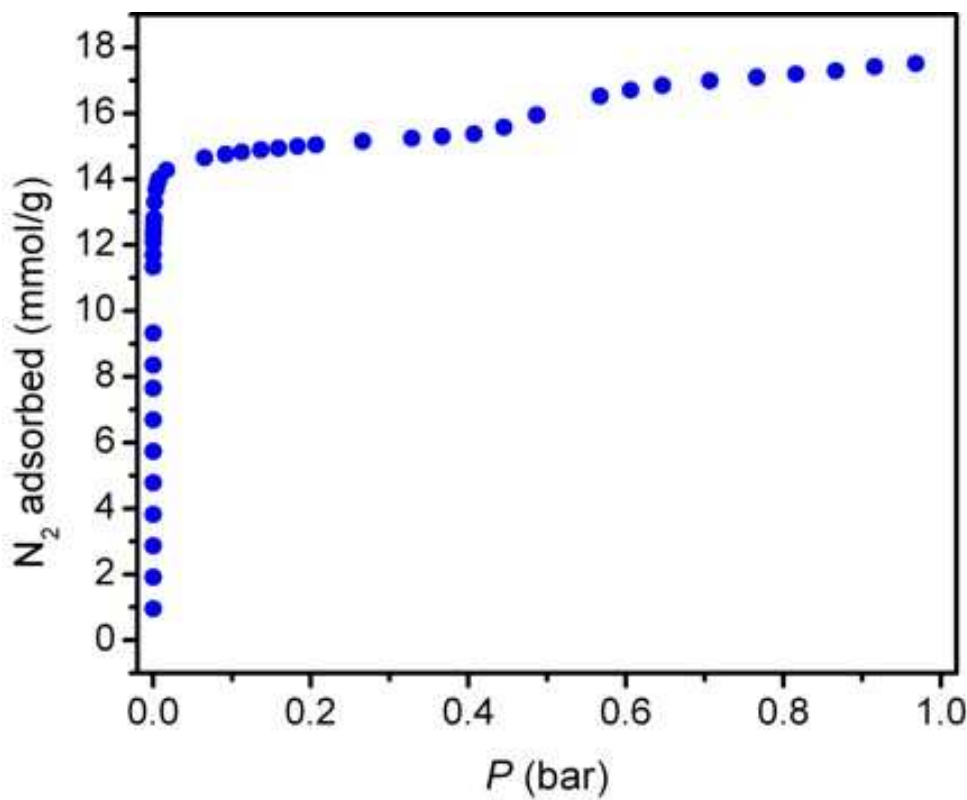


**Figure S3.**  $N_2$  adsorption in  $Fe_2(dobdc)$  at 77 K.

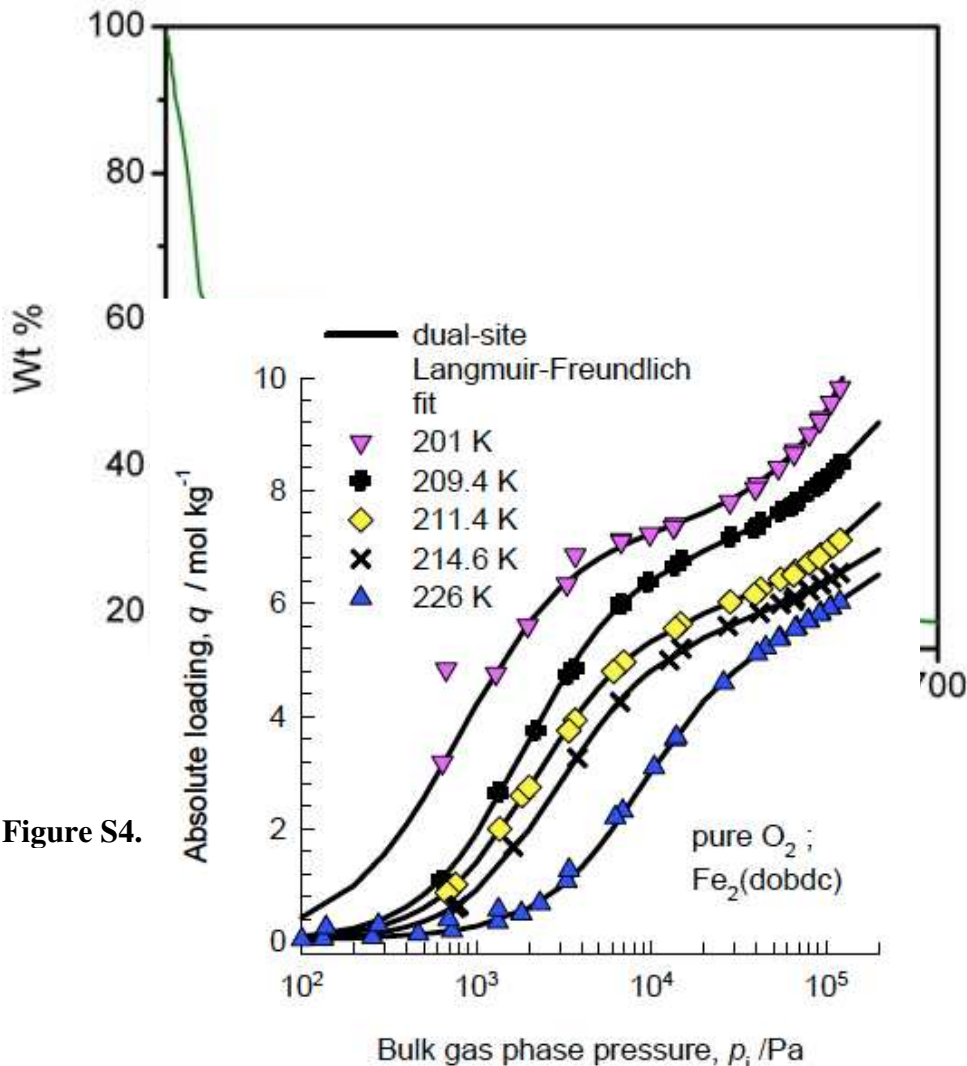


**Figure S4.**

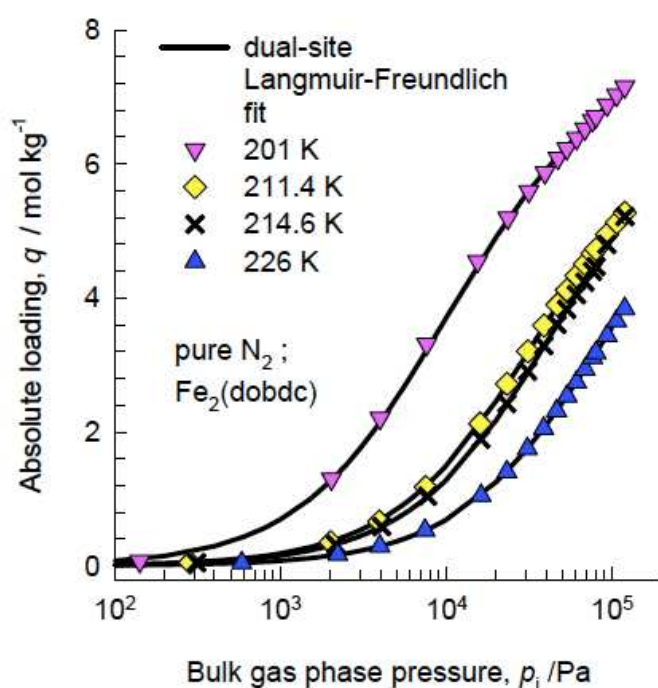


**Figure S5.** Dual-site Langmuir-Freundlich fits for Oxygen (upper) and Nitrogen (lower) adsorption in  $\text{Fe}_2(\text{dobdc})$ . The continuous solid lines are the dual-site Langmuir-Freundlich fits using the parameters specified in Table S1( $\text{O}_2$ ) and Table S2( $\text{N}_2$ )

$$\text{Absolute loading, } q \text{ / mol kg}^{-1}$$

**Figure S6.** Isosteric heats of adsorption of  $\text{O}_2$  and  $\text{N}_2$ , determined from the dual-Langmuir-Freundlich fits in Table S1, Table S2 and application of equation (2)

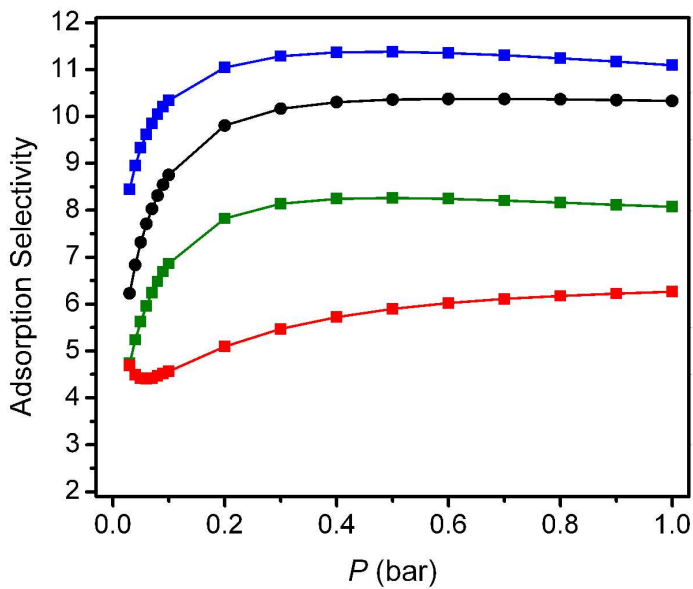


**Figure S7.**  $\text{O}_2/\text{N}_2$  selectivity as a function of pressure at 201 K (blue), 211 K (black), 214 K (green), and 226 K (red).

## Fitting of isotherms

The measured experimental data on pure component isotherms for O<sub>2</sub> and N<sub>2</sub>, in terms of excess loadings, were first converted to absolute loading using the Peng-Robinson equation of state for estimation of the fluid densities. The pore volume used for this purpose was 0.625 cm<sup>3</sup>/g.

For the O<sub>2</sub> isotherms it is particularly noteworthy there are pronounced inflections, and the inflection characteristics change with temperature; see Figure S5. For each temperature, the absolute component loadings were fitted dual-site Langmuir-Freundlich model

$$q_i = q_{i,A,sat} \frac{b_{i,A} p_i^{\nu_{i,A}}}{1 + b_{i,A} p_i^{\nu_{i,A}}} + q_{i,B,sat} \frac{b_{i,B} p_i^{\nu_{i,B}}}{1 + b_{i,B} p_i^{\nu_{i,B}}} \quad (1)$$

where we have two distinct adsorption sites A and B.

The fitted parameters for O<sub>2</sub> isotherms are specified in Table S1. Figure S5 compares the experimental data on absolute loadings of O<sub>2</sub> with the dual-Langmuir-Freundlich fits.

For N<sub>2</sub>, there are no strong inflections, and the exponents  $\nu_i$  are unit for both sites at all temperatures. The corresponding parameter fits for pure N<sub>2</sub> are provided in Table S2. Figure S5 compares the experimental data on absolute loadings of N<sub>2</sub> with the dual-Langmuir-Freundlich fits.

The isosteric heat of adsorption,  $Q_{st}$ , were calculated on the basis of the dual-Langmuir-Freundlich fits using

$$Q_{st} = RT^2 \left( \frac{\partial \ln p}{\partial T} \right)_q \quad (2)$$

The values of  $Q_{st}$  for O<sub>2</sub> and N<sub>2</sub> as a function of the molar loadings are shown in Figure S6.

## Notation

$b$	parameter in the pure component Langmuir adsorption isotherm, Pa <sup>-1</sup>
$p$	bulk gas phase pressure, Pa
$q$	molar loading of adsorbate, mol kg <sup>-1</sup>
$q_{\text{sat}}$	saturation loading, mol kg <sup>-1</sup>
$Q_{\text{st}}$	isosteric heat of adsorption, J mol <sup>-1</sup>
$R$	gas constant, 8.314 J mol <sup>-1</sup> K <sup>-1</sup>
$T$	absolute temperature, K

### *Greek letters*

$\nu_i$	exponent in the dual-Langmuir-Freundlich isotherm, dimensionless
---------	--

### *Subscripts*

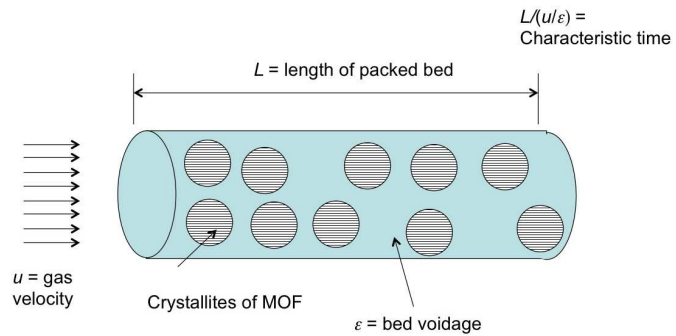
A	referring to site A
B	referring to site A
sat	referring to saturation conditions

Table S1 Dual-site Langmuir-Freundlich parameters for O<sub>2</sub> isotherms in Fe<sub>2</sub>(dobdc) at different temperatures.

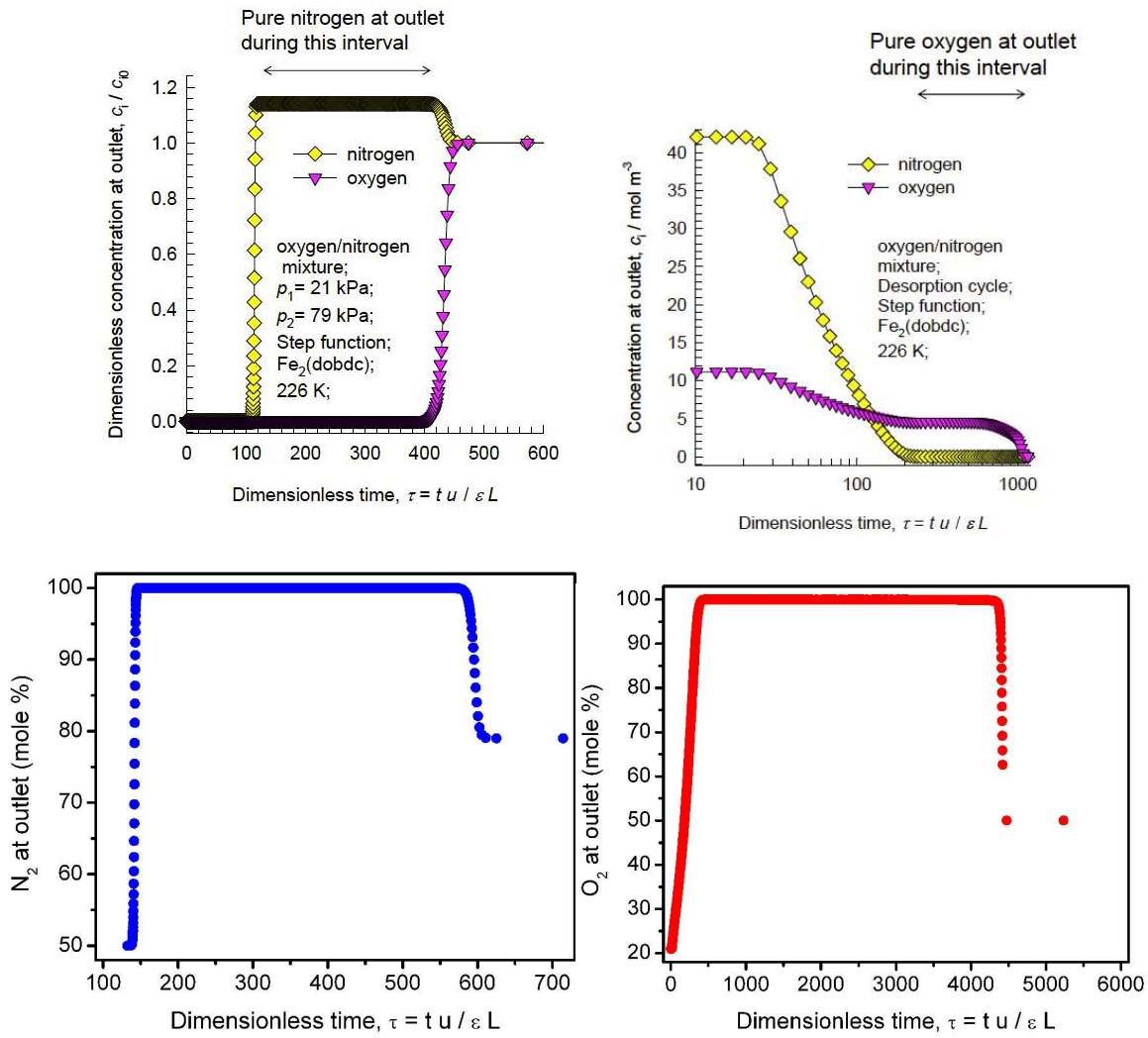
Temperature K	Site A			Site B		
	$q_{i,A,\text{sat}}$	$b_{i,A}$	$\nu_{i,A}$	$q_{i,B,\text{sat}}$	$b_{i,B}$	$\nu_{i,B}$
	mol kg <sup>-1</sup>	Pa <sup>-<math>\nu_i</math></sup>	dimensionless	mol kg <sup>-1</sup>	Pa <sup>-<math>\nu_i</math></sup>	dimensionless
201	7.26	$1.38 \times 10^{-4}$	1.33	23.86	$7.14 \times 10^{-7}$	1.03
209.4	6.62	$1.31 \times 10^{-5}$	1.49	16.71	$1.29 \times 10^{-5}$	0.78
211.4	5.62	$1.15 \times 10^{-5}$	1.48	15.58	$1.12 \times 10^{-5}$	0.78
214.6	5.34	$5.89 \times 10^{-6}$	1.51	4.23	$1.58 \times 10^{-5}$	0.87
226	4.51	$4.24 \times 10^{-7}$	1.62	33.47	$1.21 \times 10^{-4}$	0.51

Table S2. Dual-site Langmuir-Freundlich parameters for N<sub>2</sub> isotherms in Fe<sub>2</sub>(dobdc) at different temperatures.

Temperature K	Site A			Site B		
	$q_{i,A,\text{sat}}$	$b_{i,A}$	$\nu_{i,A}$	$q_{i,B,\text{sat}}$	$b_{i,B}$	$\nu_{i,B}$
	mol kg <sup>-1</sup>	Pa <sup>-<math>\nu_i</math></sup>	dimensionless	mol kg <sup>-1</sup>	Pa <sup>-<math>\nu_i</math></sup>	dimensionless
201	123.46	$4.19 \times 10^{-8}$	1	7.01	$1.09 \times 10^{-4}$	1
211.4	2.66	$3.31 \times 10^{-9}$	1	6.85	$2.81 \times 10^{-5}$	1
214.6	3.20	$3.77 \times 10^{-9}$	1	7.07	$2.22 \times 10^{-5}$	1
226	3.17	$3.75 \times 10^{-9}$	1	6.56	$1.18 \times 10^{-5}$	1



**Figure S8.** Schematic drawing of VSA apparatus.



**Figure S9.** Calculated N<sub>2</sub> breakthrough curve during adsorption of simulated air (O<sub>2</sub>:N<sub>2</sub> = 0.21:0.79) by Fe<sub>2</sub>(dobdc) at 211 K (lower left) and 226 K (upper left). Calculated O<sub>2</sub> breakthrough curve during the desorption step of the vacuum-swing adsorption process at 211 K (lower right) and 226 K (upper right)

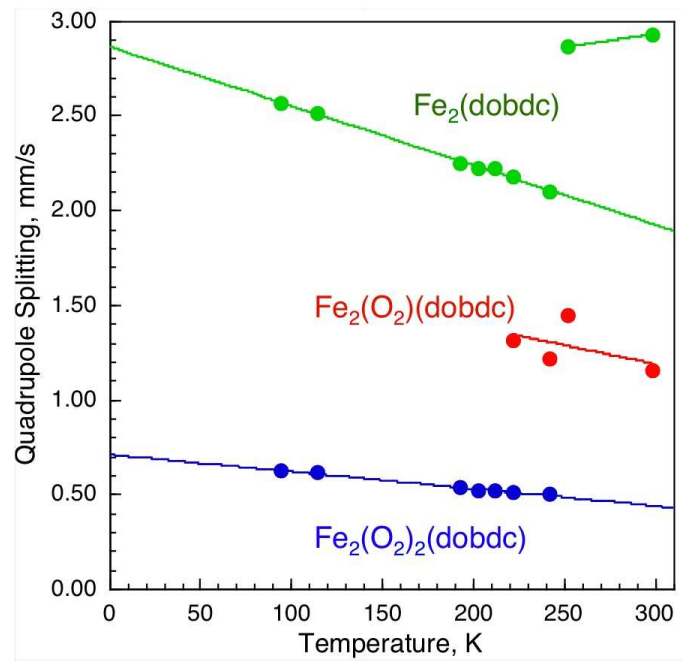


**Figure S10.** Temperature dependence of quadrupole splitting for  $\text{Fe}_2(\text{dobdc})$  (green),  $\text{Fe}_2(\text{O}_2)_2(\text{dobdc})$  (blue), and  $\text{Fe}_2(\text{O}_2)(\text{dobdc})$  red.

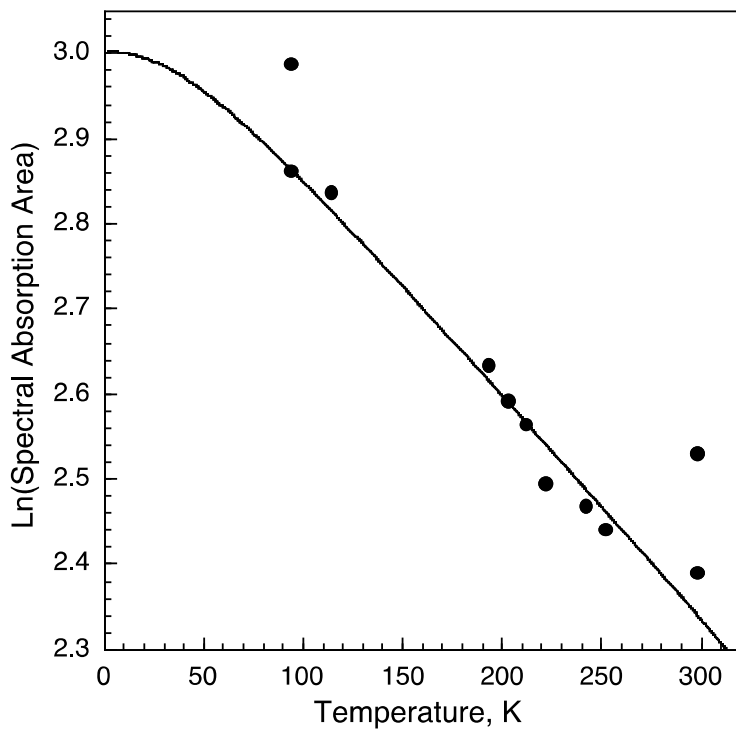


**Figure S11.** Temperature dependence of the logarithm of the Mössbauer spectral absorption area of  $\text{Fe}_2(\text{dobdc})$ .

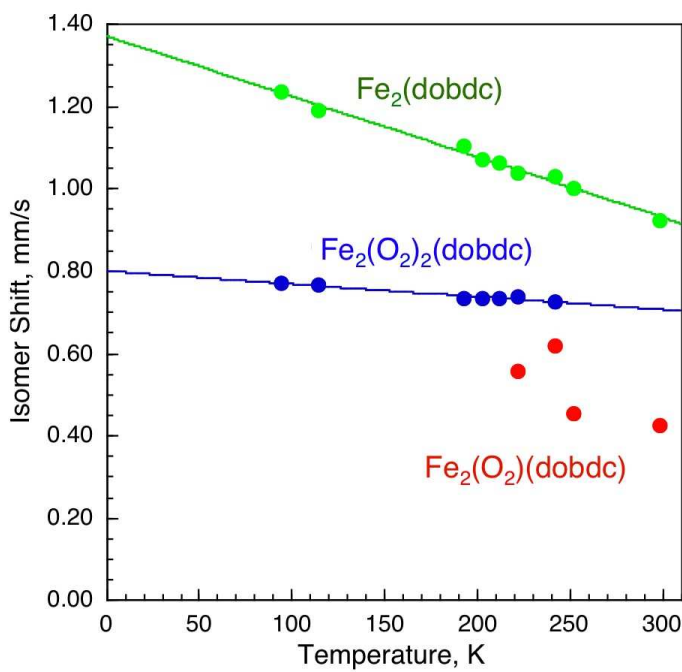


**Figure S12.** Temperature dependence of the isomer shifts  $\text{Fe}_2(\text{dobdc})$  (green),  $\text{Fe}_2(\text{O}_2)_2(\text{dobdc})$  (blue), and  $\text{Fe}_2(\text{O}_2)(\text{dobdc})$  red.

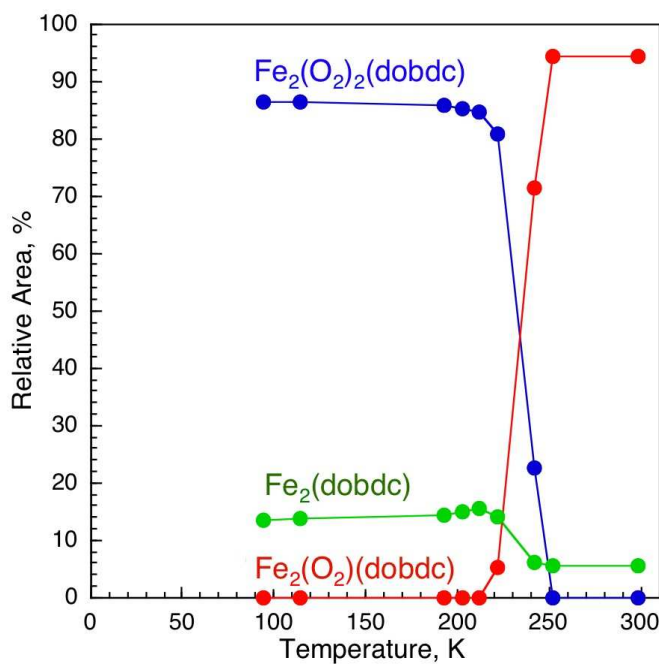
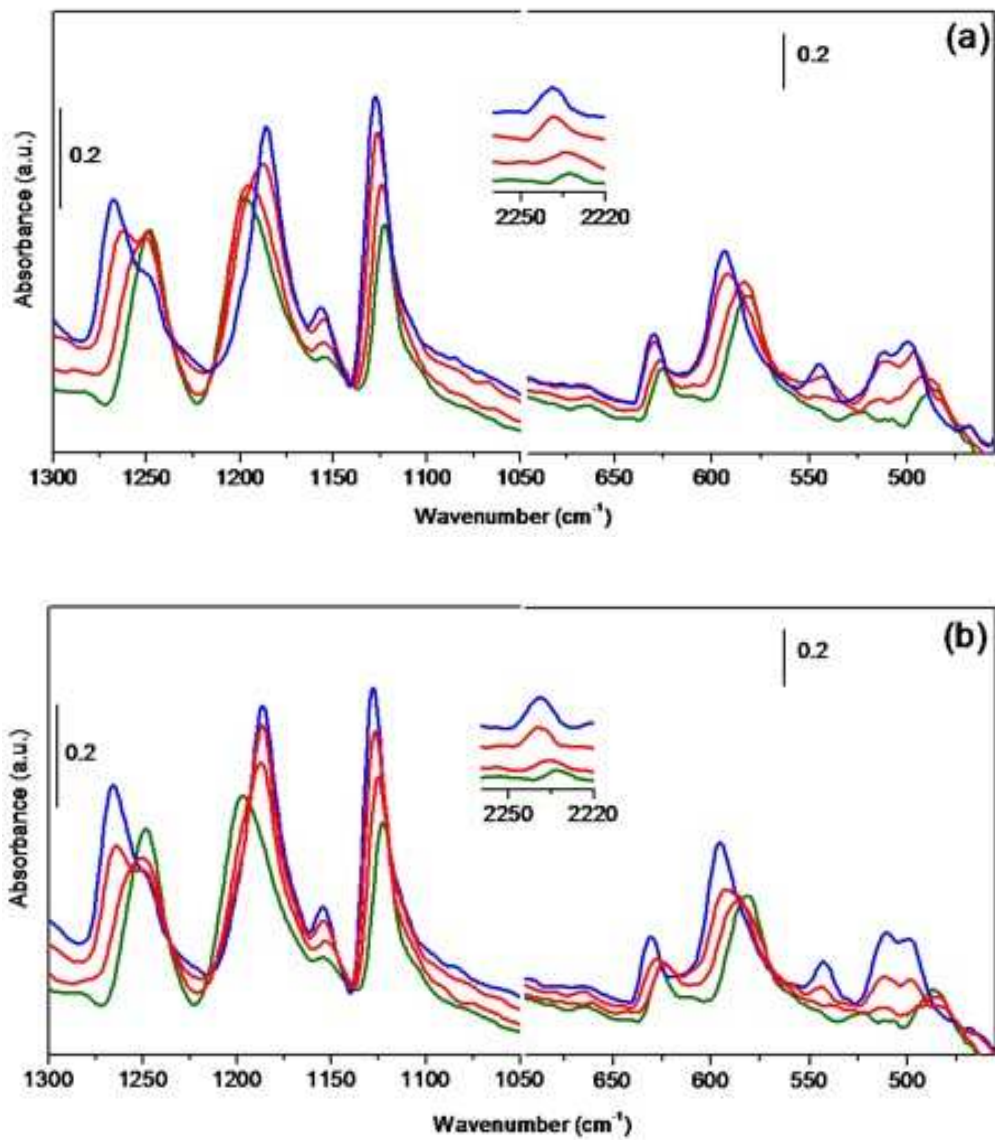


**Figure S13.** Relative absorption areas of  $\text{Fe}_2(\text{dobdc})$  (green),  $\text{Fe}_2(\text{O}_2)_2(\text{dobdc})$  (blue), and  $\text{Fe}_2(\text{O}_2)(\text{dobdc})$  (red). as a function of temperature.

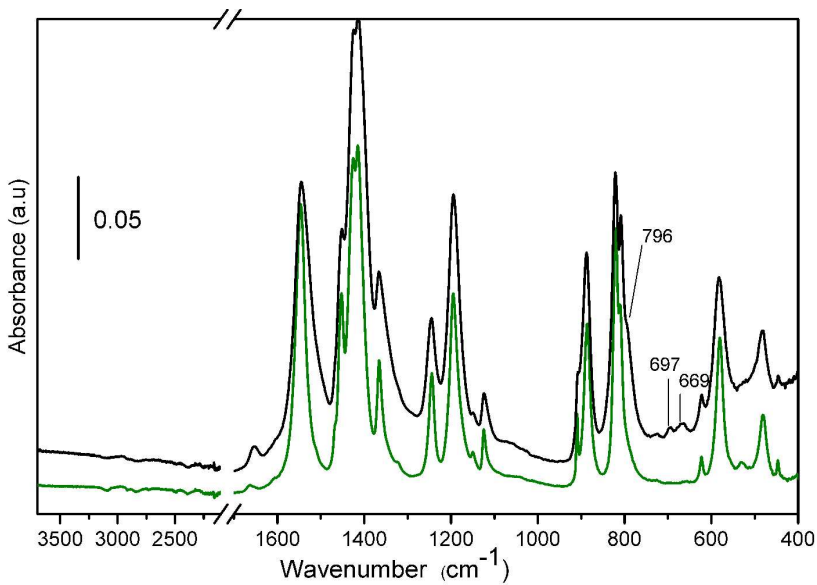
Table S3. Mössbauer Spectral Parameters for Fe<sub>2</sub>(dobdc) Obtained Before and After Oxygenation<sup>a</sup>

<i>T</i> , K	$\delta$ , mm/s <sup>b</sup>	$\Delta E_Q$ , mm/s	$\Gamma$ , mm/s	Area, %	Absolute Area, (% $\varepsilon$ )/(mm/s)	Assignment
296	1.094(3)	2.02(1)	0.30(1)	100	-	Fe <sub>2</sub> (dobdc)
94	1.208(1)	2.430(1)	0.289(1)	91.48(2)	16.09(1)	Fe <sub>2</sub> (dobdc)
	1.292(1)	2.860(1)	0.289(1)	5.12(1)	-	Fe <sub>2</sub> (dobdc)
	1.070(1)	0.219(2)	0.468(2)	3.40(1)	-	Fe <sub>2</sub> (dobdc)
45	1.223(1)	2.497(1)	0.286(2)	91.4(8)	18.1(1)	Fe <sub>2</sub> (dobdc)
	1.31(1)	2.95(2)	0.286(2)	5.4(4)	-	Fe <sub>2</sub> (dobdc)
	1.09(2)	0.24(5)	0.39(1)	3.2(3)	-	Fe <sub>2</sub> (dobdc)
94	0.772(1)	0.624(2)	0.320(2)	86.4(7)	17.50(14)	Fe <sub>2</sub> (O <sub>2</sub> ) <sub>2</sub> (dobdc)
	1.24(1)	2.57(2)	0.52(3)	13.6(7)	-	Fe <sub>2</sub> (dobdc)
114	0.768(1)	0.651(2)	0.303(2)	86.3(8)	17.06(15)	Fe <sub>2</sub> (O <sub>2</sub> ) <sub>2</sub> (dobdc)
	1.19(1)	2.51(2)	0.49(4)	13.7(8)	-	Fe <sub>2</sub> (dobdc)
193	0.734(1)	0.539(1)	0.304(1)	85.7(8)	13.93(10)	Fe <sub>2</sub> (O <sub>2</sub> ) <sub>2</sub> (dobdc)
	1.11(1)	2.24(3)	0.66(4)	14.3(8)	-	Fe <sub>2</sub> (dobdc)
203	0.732(1)	0.523(1)	0.305(2)	85.1(8)	13.35(11)	Fe <sub>2</sub> (O <sub>2</sub> ) <sub>2</sub> (dobdc)
	1.07(1)	2.22(3)	0.74(5)	14.9(8)	-	Fe <sub>2</sub> (dobdc)
212	0.735(1)	0.518(1)	0.324(2)	84.6((8))	13.00(10)	Fe <sub>2</sub> (O <sub>2</sub> ) <sub>2</sub> (dobdc)
	1.06(1)	2.22(3)	0.73(5)	15.4(8)	-	Fe <sub>2</sub> (dobdc)
222	0.55(1)	1.31(3)	0.35(5)	5.3(7)	-	Fe <sub>2</sub> (O <sub>2</sub> )(dobdc)
	0.739(1)	0.509(2)	0.318(2)	81(1)	12.11(11)	Fe <sub>2</sub> (O <sub>2</sub> ) <sub>2</sub> (dobdc)
	1.04(1)	2.18(2)	0.75(7)	14(2)	-	Fe <sub>2</sub> (dobdc)
242	0.619(5) <sup>c</sup>	1.21(2) <sup>c</sup>	0.91(3) <sup>c</sup>	71(1) <sup>c</sup>	11.80(11)	Fe <sub>2</sub> (O <sub>2</sub> )(dobdc)
	0.725(3)	0.50(2)	0.32(2)	23(1)	-	Fe <sub>2</sub> (O <sub>2</sub> ) <sub>2</sub> (dobdc)
	1.03(1)	2.10(2)	0.52(2)	6(1)	-	Fe <sub>2</sub> (dobdc)
252	0.454(1) <sup>c</sup>	1.449(6) <sup>c</sup>	0.502(4) <sup>c</sup>	94.4(3) <sup>c</sup>	11.49(4)	Fe <sub>2</sub> (O <sub>2</sub> )(dobdc)
	1.00(1)	2.87(2)	0.47(3)	5.6(3)	-	Fe <sub>2</sub> (dobdc)
298	0.415(5) <sup>c</sup>	1.24(1) <sup>c</sup>	0.41(1) <sup>c</sup>	94.4(1) <sup>c</sup>	10.91(11)	Fe <sub>2</sub> (O <sub>2</sub> )(dobdc)
	0.84(3)	2.93(6)	0.50(1)	5.6(1)	-	Fe <sub>2</sub> (dobdc)
94 <sup>d</sup>	0.497(1) <sup>c</sup>	1.200(1) <sup>c</sup>	0.389(1) <sup>c</sup>	93.6(1) <sup>c</sup>	19.83(4)	Fe <sub>2</sub> (O <sub>2</sub> )(dobdc)
	1.395(4)	2.52(1)	0.34(1)	6.4(1)	-	Fe <sub>2</sub> (dobdc)
298 <sup>d</sup>	0.427(1) <sup>c</sup>	1.153(1) <sup>c</sup>	0.388(1) <sup>c</sup>	94.4(1) <sup>c</sup>	12.56(1)	Fe <sub>2</sub> (O <sub>2</sub> )(dobdc)
	0.922(3)	2.93(1)	0.45(1)	5.6(1)	-	Fe <sub>2</sub> (dobdc)

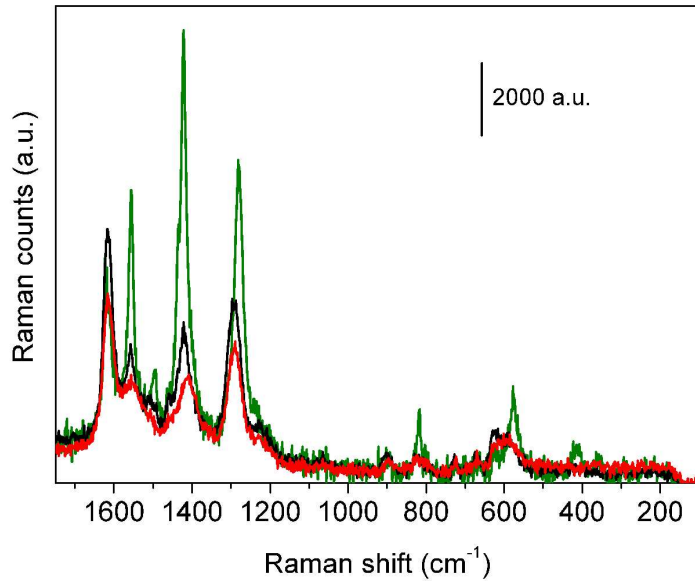
<sup>a</sup>The parameters are listed in the order of measurement and the statistical fitting errors are given in parentheses. The total errors are two to three times larger. <sup>b</sup>The isomer shifts are given relative to 295 K  $\alpha$ -iron foil. <sup>c</sup>The weighted average of or sum of the three components. <sup>d</sup>Obtained after heating to 298 K.



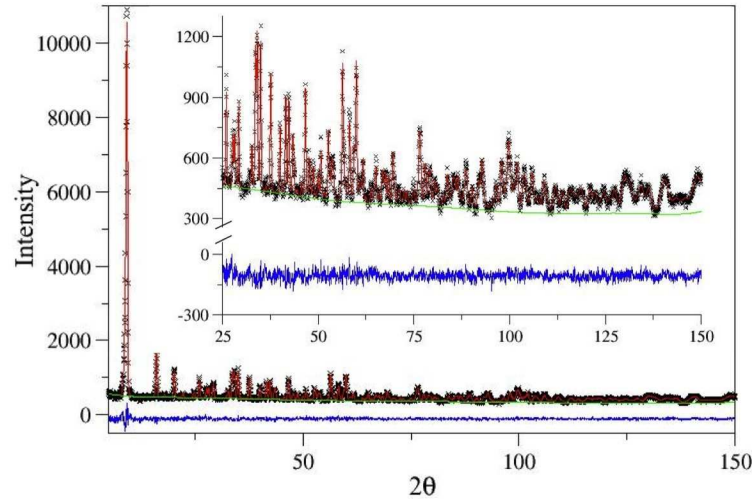
**Figure S14.** Part a): IR spectra of activated  $\text{Fe}_2(\text{dobdc})$  (green curves); effect of progressive dosage of  $\text{O}_2$  at low temperature red curves. Maximum coverage 30 mbar (blue curve); Part b) effect of outgassing at low temperature. It is evident that under these conditions the interaction with oxygen is fully reversible. As already described in the main text, bands associated to the superoxo species are clearly visible at 1129, 541 and 511  $\text{cm}^{-1}$ , while bands originally at 1250, 1198 and at 580  $\text{cm}^{-1}$ , shift to 1266, 1186 and 595  $\text{cm}^{-1}$  respectively. Animation of vibrational modes of  $\text{Ni}_2(\text{dobdc})$  homologue on optimized structure computed with CRYSTAL code, reveal that all of them are related with the C-O bonds of the linker, being the bands at 1250 at 580  $\text{cm}^{-1}$  strongly correlated. [1].



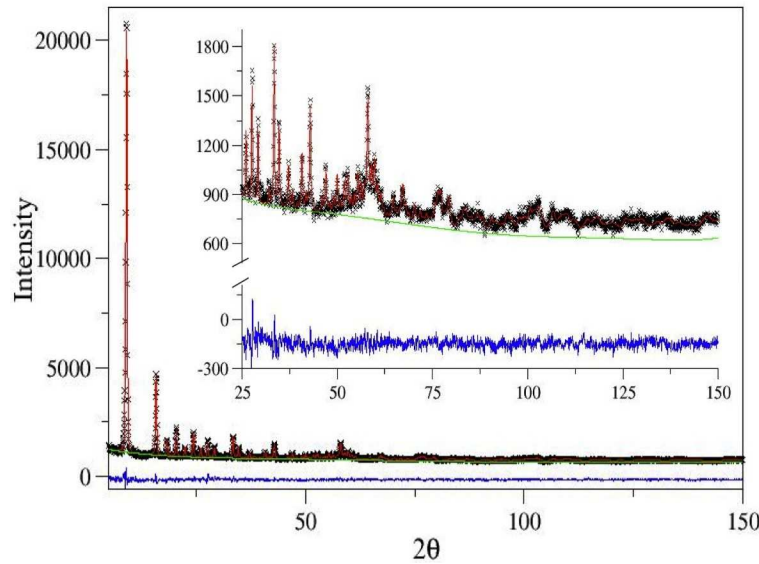
**Figure S15.** ATR spectra of activated Fe<sub>2</sub>(dobdc) (green curve); partially oxidized sample (black curve). The spectra were collected inside a N<sub>2</sub> filled glove box. Bands due to peroxy species are clearly visible at 796, 697 and 669 cm<sup>-1</sup>, confirming the data obtained in transmission mode on the sample carefully reacted at room temperature (see figure 7 of the main text).



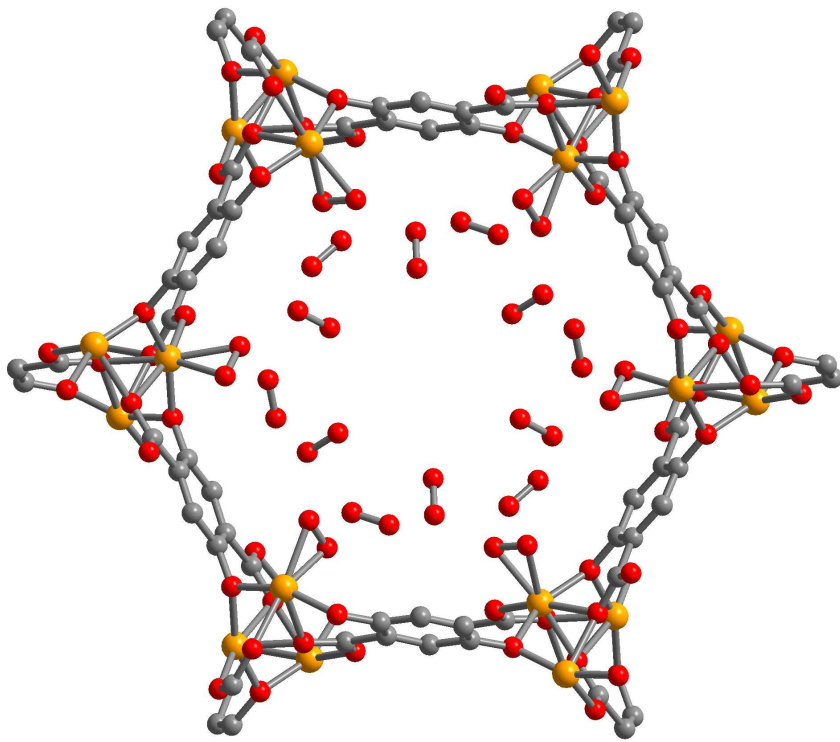
**Figure S16.** Raman spectra collected with 512 nm laser at 5% of power on sample in a cell cooled by liquid nitrogen. Spectra of activated Fe<sub>2</sub>(dobdc) (green curve); partially oxidized sample (black curve); effect of 40 mbar of oxygen on activated sample (red curve). Raman spectra have been collected on the sample cooled with a liquid nitrogen flux in order to reduce the laser damaging effects. In this case a band at 630 cm<sup>-1</sup> is the most evident feature of the formation of a peroxy species. Smaller bands at 674 and 729 are also visible. [2,3]



**Figure S17.** Rietveld refinement of the experimental neutron diffraction pattern of  $\text{Fe}_2(\text{dobdc})$  exposed to  $\text{O}_2$  at 100K. The calculated pattern (red line) is in good agreement with the experimental data (crosses) as evidenced by the difference pattern (blue line)



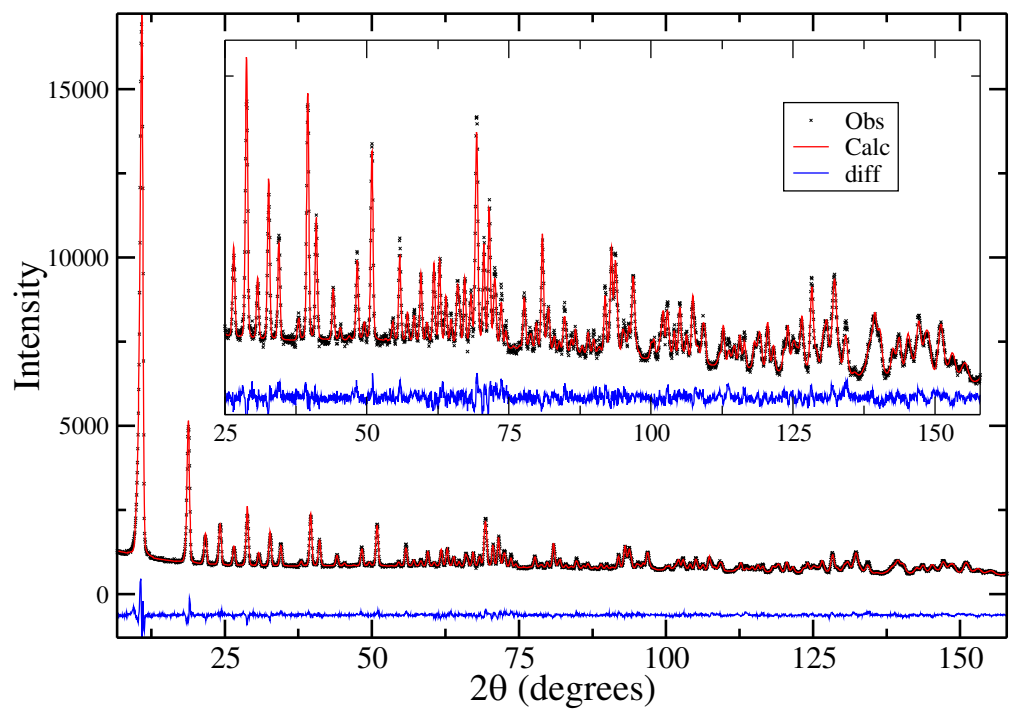
**Figure S18.** Rietveld refinement of the experimental neutron diffraction pattern of  $\text{Fe}_2(\text{dobdc})$  exposed to  $\text{O}_2$  at 298K. The calculated pattern (red line) is in good agreement with the experimental data (crosses) as evidenced by the difference pattern (blue line)



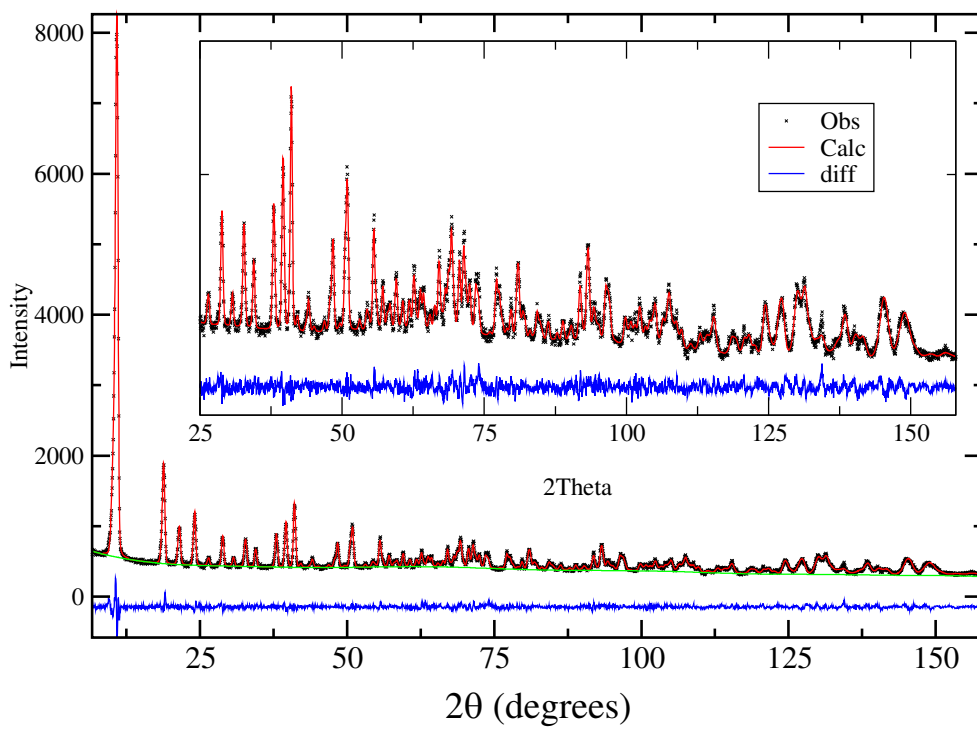
**Figure S19.** Structure of  $\text{Fe}_2(\text{O}_2)_2(\text{dobdc})\text{-}2\text{O}_2$  as viewed down the (001) direction. Orange, red, and gray atoms represent iron, oxygen, and carbon, respectively. H atoms have been omitted for clarity.

Table S4. Unit Cell lengths and volumes

	$a = b$ (Å)	$c$ (Å)	$V$ (Å)
$\text{Fe}_2(\text{dobdc})$	26.098(1)	6.8512(2)	4041.3
$\text{Fe}_2(\text{O}_2)_2(\text{dobdc})$	25.518(1)	6.9661(4)	3928.3
$\text{Fe}_2(\text{O}_2)(\text{dobdc})$	26.009(1)	6.8131(7)	3991.3
$\text{Fe}_2(\text{N}_2)_2(\text{dobdc})$	26.015(1)	6.9480(2)	4072.3



**Figure S20.** Rietveld refinement of the bare  $\text{Fe}_2(\text{dobdc})$  framework neutron diffraction data measured using Echidna. The data (crosses) are well modeled which the fitted curve (red) and difference curve (blue) indicate. Inset: magnified view of the data above  $25^\circ$ .



**Figure S21.** Rietveld refinement of the 0.5 N<sub>2</sub>:Fe neutron diffraction data measured using Echidna. Data (crosses), fit (red line), background (green line) and difference curve (blue line) indicate the quality of fits to the model described in the text.

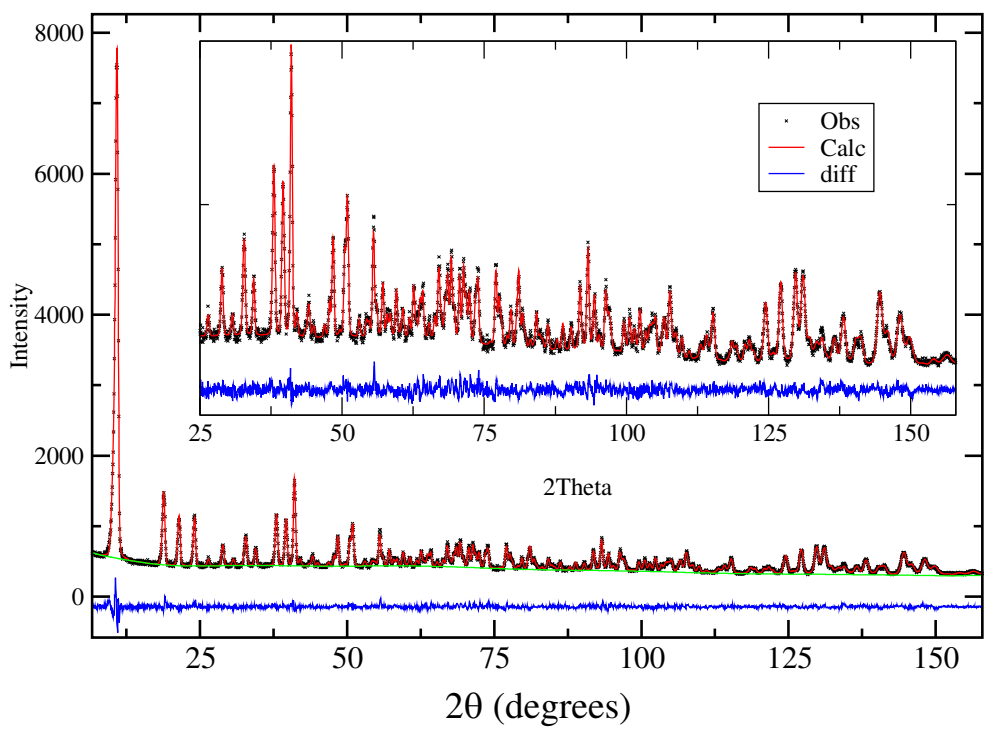


**Figure S22.** Rietveld refinement of the 1.0 N<sub>2</sub>:Fe neutron diffraction data measured using Echidna. Data (crosses), fit (red line), background (green line) and difference curve (blue line) indicate the quality of fits to the model described in the text.

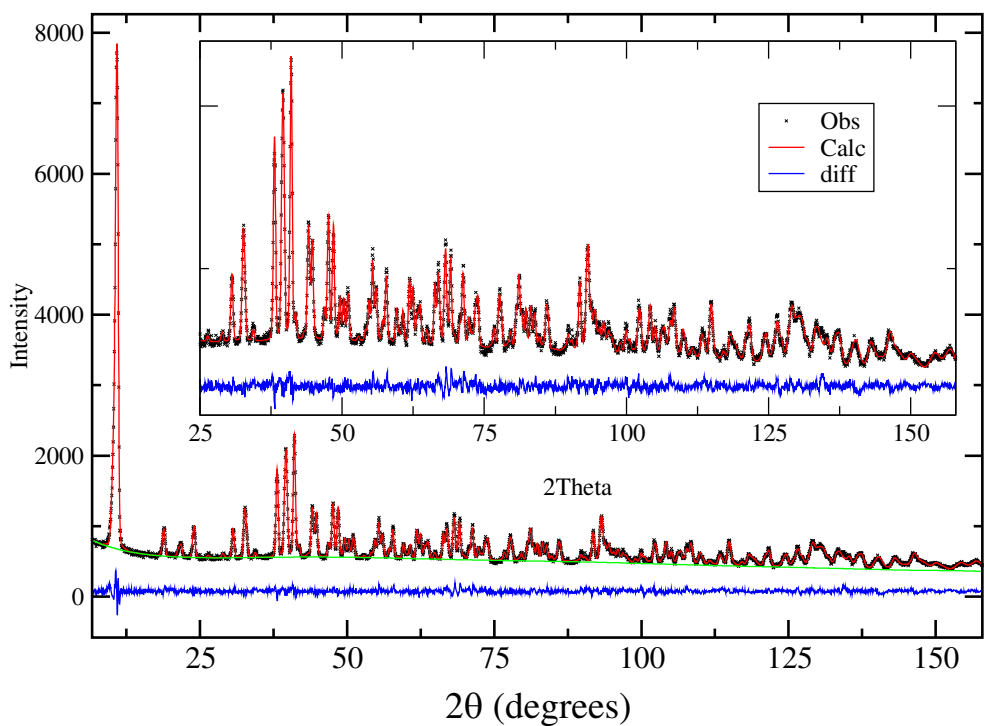


**Figure S23.** Rietveld refinement of the 2.0 N<sub>2</sub>:Fe neutron diffraction data measured using Echidna. Data (crosses), fit (red line), background (green line) and difference curve (blue line) indicate the quality of fits to the model described in the text.

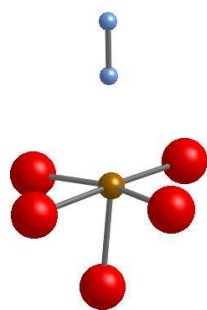


**Figure S24.** Portion of the crystal structure of the 0.5 N<sub>2</sub>:Fe loaded sample showing the end-on coordination of the nitrogen molecule (blue) to the Fe center (orange) at 2.299(13) Å. The N<sub>2</sub> intermolecular bondlength is 1.13(2) Å. Red spheres are oxygen

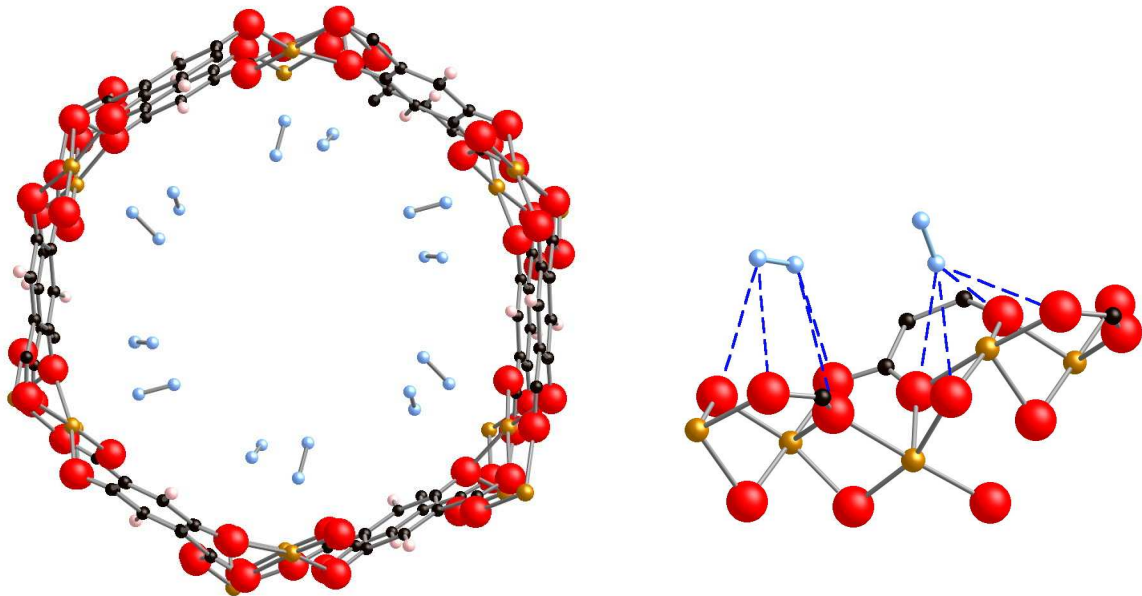


**Figure S25.** (Left) Portion of the crystal structure of the 2.0 N<sub>2</sub>:Fe loaded sample as viewed down the pore running along the crystal *c*-axis. (Right) N-O close contacts of 3.6 Å or shorter are indicated by dashed blue lines.

**Table S5:** Rietveld Refinement (9 K data) of bare Fe<sub>2</sub>(dobdc).

Space group R-3,  $a = 26.0983(5)$  Å,  $c = 6.85119(15)$  Å, cell volume = 4041.30(14) Å.

Goodness-of-fit parameters: wRp = 3.59 %, Rp = 2.82 %, reduced  $\chi^2 = 2.84$ .

Atom	X	Y	Z	Multiplicity	Occupancy	Uiso (Å <sup>2</sup> )
Fe	0.3824(2)	0.3521(2)	0.1430(6)	18	1.0	0.012(2)
O1	0.3272(3)	0.2938(4)	0.363(1)	18	1.0	0.003(3)
O2	0.3010(4)	0.2272(4)	0.599(2)	18	1.0	0.023(3)
O3	0.3551(4)	0.2732(4)	0.007(1)	18	1.0	0.009(2)
C1	0.3161(4)	0.2440(4)	0.421(1)	18	1.0	0.022(2)
C2	0.3259(4)	0.2038(3)	0.286(1)	18	1.0	0.002(2)
C3	0.3430(3)	0.2226(4)	0.095(1)	18	1.0	0.012(2)
C4	0.3487(3)	0.1819(4)	-0.034(1)	18	1.0	0.003(2)
H	0.3613(6)	0.1919(6)	-0.168(2)	18	1.0	0.01(1)

**Table S6:** Rietveld Refinement (9 K data) of 0.5 N<sub>2</sub>:Fe adsorbed in Fe<sub>2</sub>(dobdc).

Space group R-3,  $a = 26.0579(7)$  Å,  $c = 6.89634(25)$  Å, cell volume = 4055.34(21) Å.

Goodness-of-fit parameters: wRp = 4.01 %, Rp = 3.17 %, reduced  $\chi^2 = 1.89$ .

Refined 0.64 N<sub>2</sub>:Fe.

Atom	X	Y	Z	Multiplicity	Occupancy	Uiso (Å <sup>2</sup> )
Fe	0.38302(23)	0.35141(23)	0.1466(7)	18	1.0	0.015(2)
O1	0.32309(33)	0.29230(34)	0.3498(12)	18	1.0	0.005(3)
O2	0.3028(4)	0.2277(4)	0.5930(14)	18	1.0	0.022(3)
O3	0.3539(4)	0.27343(32)	0.0102(13)	18	1.0	0.003(2)
C1	0.3175(4)	0.2465(4)	0.4269(11)	18	1.0	0.025(2)
C2	0.32599(34)	0.20486(33)	0.2789(12)	18	1.0	0.016(2)
C3	0.34421(31)	0.22253(32)	0.0952(11)	18	1.0	0.011(2)
C4	0.34980(32)	0.18253(31)	-0.0320(10)	18	1.0	0.001(2)
H	0.3613	0.19194	-0.16832	18	1.0	0.01
N1	0.4636(4)	0.3489(4)	0.2709(16)	18	0.641(5)	0.036(2)
N2	0.5035(4)	0.3475(4)	0.3293(15)	18	0.641(5)	0.036(2)

**Table S7:** Rietveld Refinement (9 K data) of 1.0 N<sub>2</sub>:Fe adsorbed in Fe<sub>2</sub>(dobdc).

Space group R-3,  $a = 26.0419(4)$  Å,  $c = 6.90999(13)$  Å, cell volume = 4058.40(13) Å.

Goodness-of-fit parameters: wRp = 3.72 %, Rp = 3.01 %, reduced  $\chi^2 = 1.61$ .

Refined 0.90 N<sub>2</sub>:Fe.

Atom	X	Y	Z	Multiplicity	Occupancy	Uiso (Å <sup>2</sup> )
Fe	0.38222(17)	0.35179(17)	0.1458(6)	18	1.0	0.0084(9)
O1	0.32345(28)	0.29136(28)	0.3606(9)	18	1.0	0.004(2)
O2	0.30370(31)	0.22748(33)	0.5962(11)	18	1.0	0.017(2)
O3	0.35417(31)	0.27177(27)	0.0138(11)	18	1.0	0.010(2)
C1	0.31754(28)	0.24576(27)	0.4236(8)	18	1.0	0.014(2)
C2	0.32576(27)	0.20447(26)	0.2809(9)	18	1.0	0.013(2)
C3	0.34408(28)	0.22091(26)	0.0907(9)	18	1.0	0.020(2)
C4	0.34930(26)	0.18125(26)	-0.0309(9)	18	1.0	0.002(2)
H	0.3613	0.19194	-0.16832	18	1.0	0.01
N1	0.46488(23)	0.34775(21)	0.2732(9)	18	0.831(4)	0.015(1)
N2	0.50416(22)	0.34695(23)	0.3317(8)	18	0.831(4)	0.015(1)
N3	0.177(3)	0.256(3)	0.394(1)	18	0.070(4)	0.015
N4	0.160(3)	0.207(3)	0.277(1)	18	0.070(4)	0.015

**Table S8:** Rietveld Refinement (9 K data) of 2.0 N<sub>2</sub>:Fe adsorbed in Fe<sub>2</sub>(dobdc).

Space group R-3,  $a = 26.0151(6)$  Å,  $c = 6.94797(19)$  Å, cell volume = 4072.29(18) Å.

Goodness-of-fit parameters: wRp = 3.52 %, Rp = 2.80 %, reduced  $\chi^2 = 1.84$ .

Refined 1.76 N<sub>2</sub>:Fe.

Atom	X	Y	Z	Multiplicity	Occupancy	Uiso (Å <sup>2</sup> )
Fe	0.38366(22)	0.35294(23)	0.1457(8)	18	1.0	0.004(2)
O1	0.3234(4)	0.2944(4)	0.3675(12)	18	1.0	0.007(3)
O2	0.3061(4)	0.2288(4)	0.5906(16)	18	1.0	0.014(3)
O3	0.3534(4)	0.2731(4)	0.0096(12)	18	1.0	-0.02(3)
C1	0.3210(4)	0.2484(4)	0.4193(11)	18	1.0	0.004(2)
C2	0.32690(34)	0.20626(33)	0.2838(12)	18	1.0	0.004(2)
C3	0.34372(34)	0.2226(4)	0.0890(12)	18	1.0	0.007(2)
C4	0.34763(34)	0.1791(4)	-0.0264(12)	18	1.0	0.009(3)
H	0.3619	0.18916	-0.18382	18	1.0	0.01
N1	0.4714(4)	0.35642(33)	0.2504(11)	18	0.894(8)	0.030(2)
N2	0.50416(22)	0.34695(23)	0.3317(8)	18	0.894(8)	0.030(2)
N3	0.1664(4)	0.2038(4)	0.3356(11)	18	0.863(7)	0.044(2)
N4	0.15674(35)	0.18108(33)	0.4607(11)	18	0.863(7)	0.044(2)